Energy Storage Materials xxx (xxxx) xxx

Contents lists available at ScienceDirect

Energy Storage Materials

journal homepage: www.elsevier.com/locate/ensm

Tailored crosslinking of Poly(ethylene oxide) enables mechanical robustness and improved sodium-ion conductivity☆

Michelle L. Lehmann [a,f,1], Guang Yang [a,***,1], Dustin Gilmer [a,f], Kee Sung Han [g], Ethan C. Self [a], Rose E. Ruther [b], Sirui Ge [e], Bingrui Li [a,c], Vijayakumar Murugesan [g], Alexei P. Sokolov [a,c], Frank M. Delnick [a], Jagjit Nanda [a,d,f,**], Tomonori Saito [a,f,*]

[a] Chemical Sciences Division, Oak Ridge National Laboratory, 1 Bethel Valley Rd, Oak Ridge, TN, 37830, USA
[b] Energy and Transportation Sciences Division, Oak Ridge National Laboratory, 1 Bethel Valley Rd, Oak Ridge, TN, 37830, USA
[c] Department of Chemistry, University of Tennessee, 1420 Circle Dr, Knoxville, TN, 37996, USA
[d] Department of Chemical and Biomolecular Engineering, University of Tennessee, 1512 Middle Dr, Knoxville, TN, 37996, USA
[e] Department of Materials Science and Engineering, University of Tennessee, 1508 Middle Dr, Knoxville, TN, 37996, USA
[f] The Bredesen Center for Interdisciplinary Research and Graduate Education, University of Tennessee, 821 Volunteer Blvd, Knoxville, TN, 37996, USA
[g] Physical and Computational Sciences Directorate, Pacific Northwest National Laboratory, Richland, WA, 99352, USA

ARTICLE INFO

Keywords:
Polymer electrolyte
Poly(ethylene oxide)
Sodium-ion battery
Conductivity
Mechanical robustness

ABSTRACT

Sodium-based energy storage systems are promising candidates for electric vehicles and grid-level energy storage applications. The advancement of sodium-based energy storage systems relies on the development of high performance sodium-ion conducting electrolytes and membranes that exhibit high ionic conductivity and mechanical stability. A crosslinked poly(ethylene oxide) based polymer electrolyte was developed that demonstrates high ionic conductivity, as well as excellent mechanical stability over a wide temperature range. Ionic conductivities up to 2.0×10^{-4} S/cm at 20 °C and 7.1×10^{-4} S/cm at 70 °C are achieved for the plasticized membrane, almost four orders of magnitude greater than that of the non-plasticized membrane. The membranes are mechanically robust, and the storage modulus of the membrane is maintained at ~1 MPa from −20 to 180 °C even with the addition of plasticizer. This study provides a synthesis approach towards the design of highly ion conducting, mechanically robust gel polymer electrolytes for Na-ion batteries, non-aqueous flow batteries, and many other applications.

1. Introduction

Sodium-based energy storage systems have gained renewed interest in recent years due to the low cost and abundance of sodium compared to lithium [1]. With the ever-growing need for low cost renewable energy storage systems, sodium-based batteries are promising candidates for electric vehicles and grid-level energy storage applications [2,3]. In addition to sodium-based anodes and cathodes, the developments of high performance sodium-ion conducting electrolytes and membranes are imperative for the success of these emerging technologies [4,5]. Though much can be learned from the Li-ion field, relatively little work has been done on the development of electrolytes for Na-based energy storage systems. Compared to conventional liquid electrolytes, solid polymer electrolytes (SPEs) offer several advantages, including all solid-state device construction, good mechanical flexibility, low cost fabrication, and high ionic conductivity due to the formation of a stable gel by plasticizing

* Corresponding author. PO Box 2008, MS6210, Oak Ridge, TN, 37831-6210, USA.
** Corresponding author. PO Box 2008, MS6124, Oak Ridge, TN, 37831-6124, USA.
*** Corresponding author. PO Box 2008, MS6124, Oak Ridge, TN, 37831-6124, USA.
E-mail addresses: yangg@ornl.gov (G. Yang), nandaj@ornl.gov (J. Nanda), saitot@ornl.gov (T. Saito).
[1] Indicates equal contribution to this work.

https://doi.org/10.1016/j.ensm.2019.06.028
Received 29 October 2018; Received in revised form 13 June 2019; Accepted 19 June 2019
Available online xxxx
2405-8297/

with solvents. In addition to cost reduction, safety is a major concern for any battery technology. Electrolyte instability issues have plagued lithium ion batteries [6], and SPEs plasticized with ether-based solvents offer a safer alternative to conventional carbonate-based liquid electrolytes [7]. Poly(ethylene oxide) (PEO) has been extensively studied as a SPE due to its ability to form complexes with various cations [8–10]. However, PEO electrolytes typically exhibit poor room temperature ionic conductivity (10^{-7} – 10^{-6} S/cm) due to the semi-crystalline nature of PEO [11–14]. The addition of plasticizer to the polymer network has been shown to improve the room temperature ionic conductivity of PEO (10^{-6} – 10^{-5} S/cm) [15–17], but the weak mechanical properties of plasticized PEO prevents its use for practical applications.

Crosslinking is an effective means to increase the mechanical strength of polymer electrolytes, including PEO-based electrolytes [18,19]. In the case of linear PEO, the mechanical strength derives from the well stacked chains in the crystalline phase and chain entanglement, but it loses mechanical integrity at temperatures above the crystalline melting point at around 56 °C. Thus, several techniques have been developed to fabricate Li-ion conductive crosslinked PEO-based SPEs. Photo-induced crosslinking usually uses an ultraviolet (UV) light source to cure the precursors [20]. The curing kinetics of this technique require delicate control, and UV induced crosslinking may not be compatible with certain inorganic fillers that are commonly added to improve the SPE properties. Free radical polymerization is another crosslinking technique. However, an air-free environment is necessary to keep the radicals active and additional steps are usually necessary, such as precursor degassing and polymer purification [21]. On the other hand, thermally induced polymerization can be effectively used to crosslink the precursors [22]. The precursor mixture is thermally processed below the thermal decomposition temperature of all components, possibly also in solvent free surroundings. Also, this method allows for precise control over crosslink density, which is determined by the precursor chain length and readily tunable. Therefore, membrane fabrication with thermally induced polymerization is ideal for scale up with high efficiency, high yield, and ease of control.

To date, several crosslinked PEO-based membranes have been studied for lithium systems [18,23–26], but few reports exist on gel polymer electrolytes for sodium systems. Gao et al. [27]. reported a radical polymerized crosslinked poly(methyl methacrylate)-tetraethylene glycol dimethyl ether (TEGDME) gel polymer electrolyte for a sodium-sulfur battery that exhibited excellent electrochemical stability, though it required a cellulose layer for mechanical support. Colo et al. [28] reported a photo-crosslinked PEO-based polymer that demonstrated excellent conductivity (1×10^{-3} S/cm) at room temperature; however, this is above the crystalline melting temperature and no room temperature mechanical properties were reported. Bella et al. [29] reported a poly(ethylene glycol methyl ether methacrylate) crosslinked polymer electrolyte plasticized with a 1 M solution of $NaClO_4$ in propylene carbonate. The photo-crosslinked polymer also displayed excellent room temperature conductivity (5.1×10^{-3} S/cm) but showed extensive swelling (200%) when immersed in the electrolyte. Further advancement of mechanically robust and highly Na-ion conductive membranes is necessary to meet the future demand of the technology. This is especially true for non-aqueous flow battery applications, which require mechanical stability while fully immersed in liquid electrolyte.

Herein we demonstrate a facile single step synthesis approach that utilizes readily available building blocks to create a mechanically robust crosslinked PEO membrane for Na-based batteries. The PEO-based polymer is designed to be highly crosslinked, providing mechanical robustness over a wide temperature range and when completely immersed in electrolyte. Even with a high degree of crosslinking, the membrane remains flexible and completely amorphous, which imparts excellent ionic conductivity at room temperature. We utilize TEGDME as a plasticizer due to its compatibility with PEO as well as its excellent electrochemical and thermal stability [7,30,31]. TEGDME is more stable with respect to reduction than carbonate solvents and is thermally stable to just below 200 °C. The role of ethylene oxide (EO) complexation with sodium triflate (NaTf) and its effect on polymer segmental dynamics and ionic conductivity is elucidated with and without TEGDME as a plasticizer. The mechanical properties of the crosslinked membrane are evaluated using dynamic mechanical analysis (DMA) and rheology.

2. Experimental

2.1. Materials

The crosslinked PEO membrane contained two polymer precursors: (i) Poly(ethylene glycol) diglycidyl ether (PEGDGE, Sigma Aldrich, $M_n = 500$ g/mol) and (ii) Jeffamine® ED 900 (95% purity, Huntsman, $M_n = 900$ g/mol), a diamine with a poly(ethylene glycol) and poly(-propylene glycol) backbone. Poly(ethylene oxide) (PEO, Sigma Aldrich, $M_v = 600{,}000$ g/mol) was used as the linear PEO reference, and sodium trifluoromethanesulfonate (sodium triflate, NaTf, 98%, Sigma Aldrich) was the salt in all membranes. Diethylene glycol dimethyl ether (diglyme, 99.5%, Sigma Aldrich) was used to cast the crosslinked membranes. All reagents used in the preparation of crosslinked films were used as received, except for TEGDME (≥99%, Sigma Aldrich) which was dried over molecular sieves and stored in an inert atmosphere.

2.2. Film preparation

Crosslinked films were prepared using a solution-casting technique where the NaTf concentration was varied with respect to the polymer from 8 to 40 wt%. The molar ratio of epoxides in PEGDGE to amines in Jeffamine was fixed at 2:1 for all films. The polymers were mixed using a magnetic stir bar for 24 h before adding the desired amount of NaTf (dissolved in 5 ml diglyme). The polymer/solvent/NaTf mixture was mixed for 3–5 h to allow for complexation of the salt with the polymer chains. The resulting solution was cast in a Teflon® dish and cured at 100 °C for 3–3.5 h. All the fabricated membranes were dried under vacuum for 24 h at room temperature to remove any residual solvent. Plasticized samples were prepared in an Ar-filled glove box by soaking the dry membranes in excess TEGDME for 24 h and blotting dry. The initial and final mass of the samples were measured to determine the amount of TEGDME incorporated into the film (Table S2). All plasticized membranes contained approximately 50 wt% TEGDME. Residual TEGDME from plasticization was evaporated to dryness, and no evidence of NaTf was observed, indicating the TEGDME soaking procedure did not leach NaTf salt from the polymer membrane.

Linear PEO-NaTf membranes were made as follows. The butylated hydroxytoluene (BHT) inhibitor in linear PEO was removed by rinsing 5 g PEO with 1 L of acetone, followed by drying PEO ($M_v = 600{,}000$ g/mol) at 60 °C under vacuum for a minimum of 24 h. NaTf was dried under vacuum at 90 °C for 8 h. PEO and NaTf were dissolved in acetonitrile (Sigma Aldrich, anhydrous, 99.8%) to form 4 wt% and 3 wt% stock solutions, respectively. These two stock solutions were mixed to form a series of PEO-NaTf solutions, with NaTf concentrations ranging from 12 wt% to 40 wt% in the final membrane. One plasticized linear PEO-NaTf sample was prepared by adding 2 mol of TEGDME per 1 mol EO to the solution. The PEO-NaTf solution was then cast into a Teflon® dish and dried under ambient conditions for 8 h, followed by a 16 h drying step under vacuum to evaporate any residual acetonitrile. All membranes were stored in an Ar-filled glove box ($H_2O < 0.1$ ppm, $O_2 < 0.1$ ppm) for further use.

2.3. Electrochemical characterizations

Ionic conductivity of the membranes was measured by electrochemical impedance spectroscopy. Samples were punched into circular disks (1.27 cm in diameter) and sealed between two stainless-steel electrodes using heat shrink tubing to prevent moisture exposure during measurements. The impedance for each film was measured at

multiple temperatures (20–70 °C) over a frequency range of 10^6–1 Hz using a 6 mV AC signal. Samples were thermally cycled three times between 20 and 70 °C in 10 °C increments to ensure reproducibility in the impedance measurements. All samples for electrochemical measurements were prepared in a glovebox and were performed using a Biologic VMP3 potentiostat and EC-Lab® software. The electrochemical stability window and Na^+ transference number of dry and TEGDME plasticized 18 wt% NaTf membranes were measured at 40 °C, with an additional transference number measurement at 20 °C with a plasticized membrane. The electrochemical stability window was measured using sodium foil as the counter and reference electrodes with a stainless-steel working electrode by linear sweep voltammetry between open circuit voltage and 6 V (*vs.* Na^+/Na) at a rate of 10 mV per second. For transference number measurements, a sodium foil symmetric cell was used, and a small DC potential of 7.5 mV was applied, and the current decay was monitored over time. Electrochemical impedance spectra at open circuit voltage just before applying the bias potential and after the current reached a steady state value were measured. Sodium stripping and plating stability test was performed at 40 °C using a sodium foil symmetric cell and a TEGDME plasticized 18 wt% NaTf crosslinked PEO and 18 wt% NaTf Linear PEO, cycled at a 73 μA/cm^2 current density.

2.4. Thermal characterizations: determination of glass transition temperature, melting temperature and thermal profile

Glass transition temperature (T_g) and melting temperature (T_m) of each membrane were measured using differential scanning calorimetry (DSC, TA instruments Q2000). Samples were sealed in aluminum DSC pans in an argon atmosphere prior to measurement. The samples were cycled at a rate of 5 °C/min from −90 to 90 °C for 2 cycles, and T_g and T_m were recorded from the second cycle. The thermal profile of dry and TEGDME plasticized membranes were performed by thermal gravimetric analysis (TGA, TA Instruments Q50). TGA was conducted under nitrogen from 25 to 800 °C at a heating rate of 20 °C/min.

2.5. Mechanical analysis

Films were fabricated into approximately $(9 \times 4 \times 0.1)$ mm^3 specimens for mechanical analysis. Storage and loss modulus were measured by dynamic mechanical analysis (DMA) at an operating frequency of 1 Hz utilizing a TA Instruments RSA-G2 Solids Analyzer as the samples were heated from 20 °C to 200 °C at 3 °C/min under nitrogen. Tensile measurements were performed according to ASTM D1708 using an Instron 3343 universal tensile meter. Membranes were stretched at a constant rate of 1 mm/min at room temperature in air until break. Reported tensile properties are an average of 5 samples.

2.6. Shear rheology

Mechanical transitions in linear and crosslinked PEO samples were measured utilizing an AR2000ex rheometer (TA instruments) through temperature sweep tests in an oscillatory shear mode under a nitrogen atmosphere. Two different geometries were applied based on the magnitude of the shear modulus. The temperature range was −60 to 180 °C for the crosslinked PEO sample and −40 to 180 °C for the linear PEO sample. For both samples, the temperature ramp rate was 1 °C/min, and the angular frequency was 1 rad/s. Parallel plates (4 mm in diameter) were employed for measuring the crosslinked PEO sample over the entire temperature range. For the linear PEO sample, parallel plates of 4 mm diameter were used from −40 to 45 °C, and parallel plates of 8 mm diameter were used from 45 to 180 °C. The stress controlled oscillatory mode was set to 25,000 Pa stress for the entire temperature range for the crosslinked PEO sample. For linear PEO, the stress controlled oscillatory mode was set to 25,000 Pa stress for the temperature range of −40 to 45 °C, and the strain controlled mode was set to 0.15% strain for the temperature range of 45–180 °C.

2.7. Fourier-transform infrared spectroscopy (FTIR)

IR spectra were collected with a FTIR spectrometer (Bruker, ALPHA) using a diamond attenuated total reflection (ATR) accessory. The IR measurements were performed in an argon-filled glove box with O_2 and $H_2O < 0.1$ ppm.

2.8. Scanning electron microscopy (SEM) and energy-dispersive X-ray (EDX) spectroscopy

Scanning electron microscope (SEM) micrographs were captured by a cold-cathode field emission (FE) SEM system (Hitachi TM3030Plus Tabletop Microscope) at 15 kV accelerating voltage. The energy dispersive X-ray spectrometer (EDX) were used to obtain the elemental composition distribution of the Na anode surface (15 kV).

2.9. Nuclear magnetic resonance (NMR)

For the determination of the ion rotational correlation time, τ_c for Na^+ cation and Tf^- anion, ^{23}Na, and ^{19}F nuclear relaxation times were measured on a 600 MHz solid state NMR spectrometer (Bruker, Germany) equipped with a 2.5 mm magic angle spinning (MAS) probe at 20 °C without spinning the samples. Spin-spin (T_2) and spin-lattice (T_1) relaxation times were determined using a Carr-Purcell-Meiboom-Gill (CPMG) (90°- τ - 180° - τ - acquisition) and the inversion-recovery (180°-τ-90°-acquisition) sequences, respectively. Larmor frequencies (ω_0) for ^{19}F and ^{23}Na relaxation measurements were $2\pi \cdot 564.644$ and $2\pi \cdot 158.751$ rad MHz, respectively. The rotational correlation time, τ_c (s) for Tf^- anion and Na^+ cation was estimated from the nuclear relaxation ratio using equation (1) [32].

$$T_2/T_1 = \left[\frac{2}{1+\omega_0^2\tau_c^2} + \frac{8}{1+4\omega_0^2\tau_c^2}\right] \Big/ \left[3 + \frac{5}{1+\omega_0^2\tau_c^2} + \frac{2}{1+4\omega_0^2\tau_c^2}\right] \quad (1)$$

From the measured τ_c, the diffusion coefficient of Na^+ cation and Tf^- anion were determined using the Einstein-Smoluchowski equation (see supporting information) [33].

3. Results and discussion

3.1. Fabrication of PEGDGE/Jeffamine crosslinked membranes

Crosslinked membranes were prepared via a single step synthesis using amine and epoxide terminated PEO-based precursors (Jeffamine, $M_n = 900$ g/mol and PEGDGE, $M_n = 500$ g/mol, respectively). The primary amine on Jeffamine reacts with the epoxide on PEGDGE to form a covalent linkage, and the resulting secondary amine further reacts to form a crosslinked network (Fig. 1a and b). The molar ratio of epoxides:amines was fixed at 2:1 to form a robust, highly crosslinked network. Constraining the PEO segments in a crosslinked network is anticipated to reduce the crystallinity associated with linear PEO. All membranes are flexible and translucent (Fig. 1c). The membranes are mechanically stable, even with the addition of plasticizer and became slightly stiffer with increasing NaTf concentration. To evaluate the effect of NaTf concentration on their T_g and ionic conductivity, the membranes were prepared with NaTf concentrations ranging from 8 to 40 wt% with respect to polymer mass (EO/Na = 32 to 4).

3.2. Impact of NaTf and TEGDME on T_g of PEGDGE/Jeffamine crosslinked membranes

Fig. 2a shows the DSC curves for non-plasticized crosslinked membranes with linear PEO shown for comparison. All crosslinked membranes exhibit a single T_g and no melting peak, which indicates suppression of PEO crystallization. In comparison, linear PEO with 34 wt % NaTf shows a T_g at −30 °C and a crystalline melting temperature (T_m)

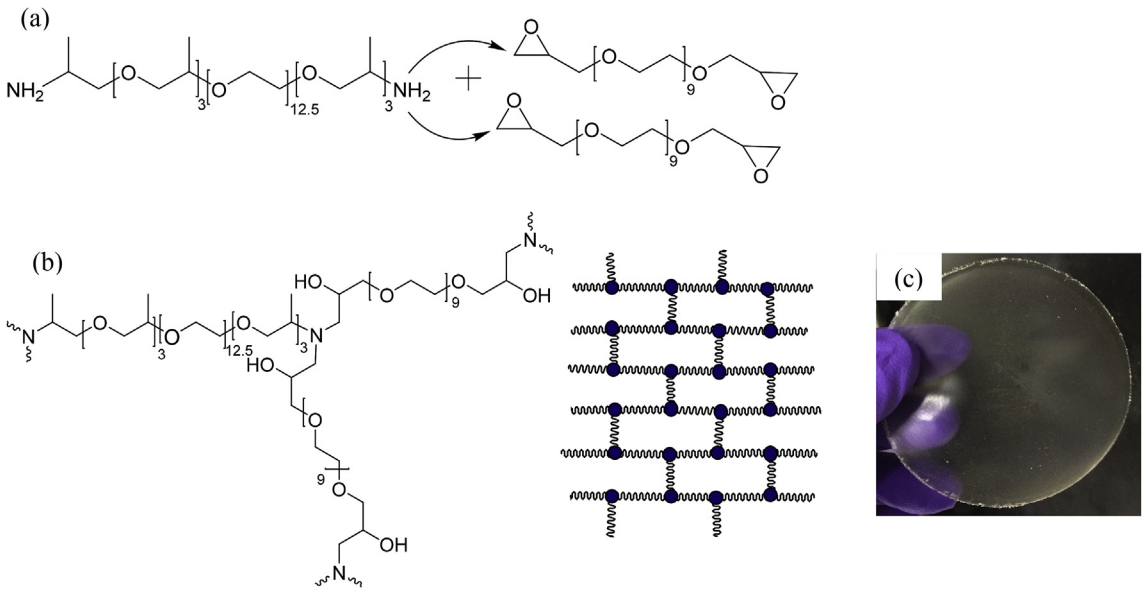

Fig. 1. (a) Reaction scheme of PEGDGE and Jeffamine to produce a crosslinked PEO-based network. (b) Schematic of a crosslinked PEO network where dots represent nitrogen and lines represent PEGDGE and Jeffamine. (c) photograph of a free standing crosslinked membrane containing 24 wt% NaTf.

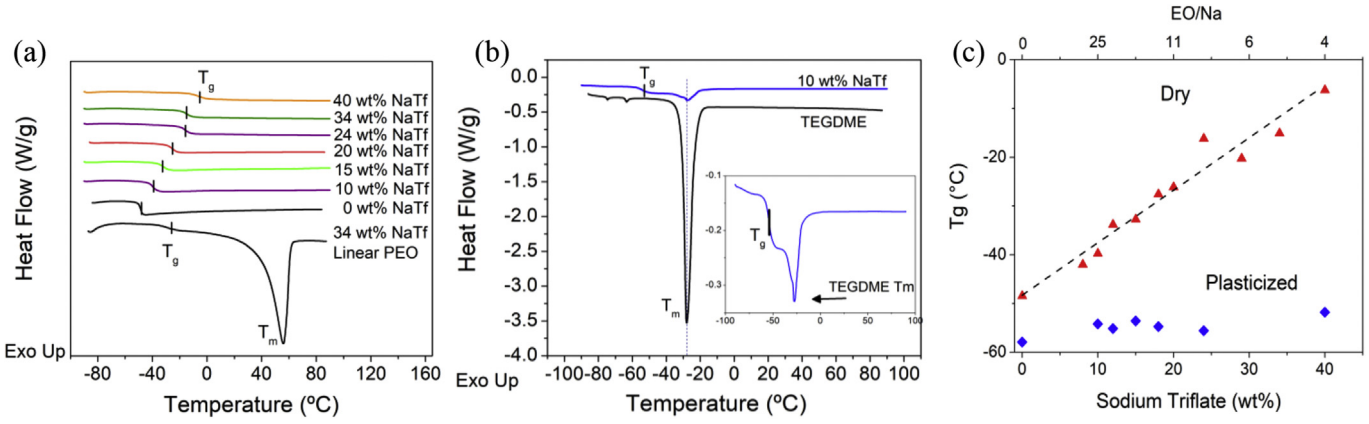

Fig. 2. (a) DSC plots for non-plasticized crosslinked and linear PEO. (b) DSC plot for 10 wt% NaTf crosslinked PEO plasticized with TEGDME. Pure TEGDME is shown for reference. Insert shows an enlarged view of T_g and T_m of plasticized 10 wt% NaTf crosslinked PEO. (c) Effect of NaTf concentration in the membrane on T_g for non-plasticized and plasticized crosslinked membranes.

of 56 °C. T_g of the dry crosslinked membranes linearly increases with NaTf concentration from −48 °C at 0 wt% to −6 °C at 40 wt% (Fig. 2c, Table S1). These results are consistent with the report by He et al. [34] for a non-plasticized crosslinked PEO-Lithium bis(trifluoromethanesulfonyl) imide (LiTFSI) electrolyte. The increase in T_g and broadening of the glass transition for dry samples is attributed to ion-dipole interactions between the Na^+ and the ether oxygens on PEG segments [15,35]. These ion-dipole interactions act as physical crosslinks within the matrix which increases T_g. This conclusion is further supported by the depression of T_g for plasticized samples, which remains fairly constant at ca. −54 °C (Fig. 2c and Table S2), as TEGDME solvates the ions, reducing the ether oxygen-Na^+ interactions. T_g of the plasticized sample containing no salt is slightly lower at −58 °C, indicating that there are some weak interactions between EO and Na^+ in the plasticized membranes that also prevents leaching of the salt during plasticization. As shown in Fig. 2b, both pure TEGDME and TEGDME incorporated into the polymer network exhibit a melting temperature of -28 °C. The percent crystallinity of TEGDME is significantly reduced when incorporated into the polymer network. Pure TEGDME is 60% crystalline, and the crystallinity of TEGDME in 1M NaTf-TEGDME is 38%. TEGDME crystallinity is reduced to roughly 8% in the membrane, indicating that the Na^+ ion forms physical crosslinks between TEGDME EO and polymer EO units, preventing TEGMDE from forming a crystalline phase. This conclusion is further supported by the slight increase in T_g for the plasticized sample with the highest salt concentration.

3.3. Ionic conductivity of PEGDGE/Jeffamine crosslinked membranes

The ionic conductivity of crosslinked and linear PEO membranes containing up to 40 wt% NaTf were measured over 20–70 °C using AC impedance spectroscopy. As shown in Fig. 3a, the ionic conductivity of the non-plasticized crosslinked PEO membranes decreases with increasing salt concentration. The slope of log(conductivity) vs. reciprocal temperature shows no significant change, indicating that there is no phase change of the polymer, which is consistent with the DSC measurements. In principle, the ion conduction mechanism in a polymer electrolyte is based on the coupling between ion transport and the segmental relaxation of the polymer chains. Increasing NaTf concentration reduces the polymer segmental motion in the dry samples (indicated by higher T_g shown in Fig. 2c), which causes a decline in ionic conductivity. The highest conductivity for the non-plasticized membranes is 6.4×10^{-5} S/cm at 70 °C for the 10 wt% NaTf sample (Fig. 3a), which is

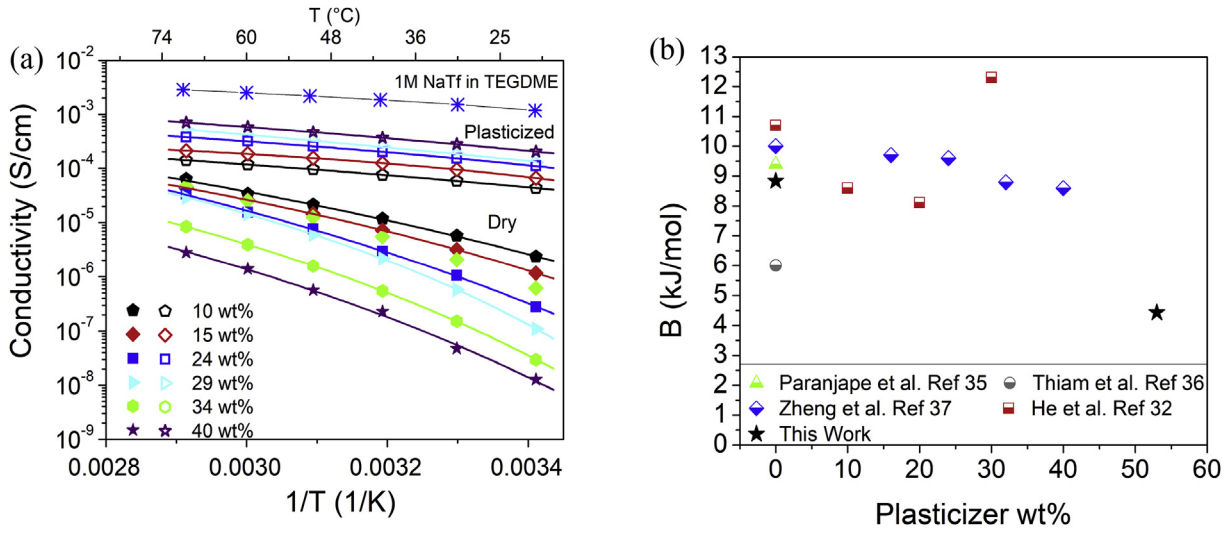

Fig. 3. (a) Conductivity as a function of temperature for selected wt% NaTf crosslinked PEO membranes. Lines indicate fit to the VFT model. 1 M NaTf in TEGDME (liquid electrolyte) is included for reference. (b) VFT parameter B of this work compared with previous reports as a function of plasticizer wt%, at a salt concentration of ~12 wt% (EO:M^+ = 20:1 where M = Li or Na).

in agreement with other PEO-based crosslinked systems using LiTFSI [34]. Unlike the dry samples, the conductivity of the plasticized films increases with increasing NaTf concentration (Fig. 3a), while T_g remains fairly constant (Fig. 2c). An increase in conductivity with ion concentration is expected at constant T_g. Overall, plasticization results in a nearly four orders of magnitude increase in ionic conductivity at room temperature for the crosslinked membrane containing 40 wt% NaTf, consistent with conductivity values reported by Kim et al. for a polyvinylidene-fluoride-*co*-hexafluoropropylene (PVDF-HFP)/TEGDME/-NaTf composite system [36].

As shown in Fig. 3a, the ionic conductivity over 20–70 °C for these crosslinked PEO-based polymers can be fit well to the Vogel-Fulcher-Tammann (VFT) equation [37]:

$$\sigma = \sigma_0 \exp\left(\frac{-B}{R(T - T_0)}\right) \quad (2)$$

where σ is the conductivity, σ_0 is the pre-exponential factor, and B and T_0 are the VFT parameters (values shown in Tables S1 and S2). The VFT parameter B for dry membranes (8.8–12 kJ/mol) is similar to those for other PEO-based crosslinked systems (6.0–10 kJ/mol) [27,38–40]. Parameter B for plasticized membranes is highly dependent upon the wt % of plasticizer within the membrane. A comparison of VFT parameter B versus plasticizer wt% for a fixed salt concentration of ~12 wt% (EO:M = 20:1) can be found in Fig. 3b. The VFT parameter B for the plasticized membranes in this work (~4 kJ/mol) is lower than other reported values (Fig. 3b) and is closer to that of 1M NaTf in TEGDME (1.8 kJ/mol) than that of the dry membranes (~9 kJ/mol), an indication that ion conduction is preferentially through TEGDME, and governed by salt-TEGDME interactions in preference to salt-polymer interactions [17].

To determine the impact of crosslinking on conductivity, crosslinked and linear PEO membranes containing various NaTf concentrations were compared. The conductivity of crosslinked and linear PEO with 12 wt% NaTf is shown in Fig. 4a as a function of temperature. Linear PEO exhibits a sharp decrease in conductivity at T < 60 °C due to crystallization, whereas the conductivity of the crosslinked membrane shows no significant change in slope over the same temperature range. At 20 °C, the ionic conductivity of the crosslinked membrane is almost an order of magnitude greater than that of linear PEO (1.6×10^{-6} vs. 4.1×10^{-7} S/cm, respectively). As seen in Fig. 4b, the conductivity for non-plasticized crosslinked membranes strongly decreases above 10 wt% NaTf concentration, while linear PEO exhibited a maximum conductivity around 20 wt% NaTf. The optimal salt concentration for the highest ionic conductivity shifted from 20 wt% NaTf for linear PEO to 10 wt% NaTf for crosslinked PEO. It should be noted that the conductivity obtained for a given polymer electrolyte depends on many factors such as the polymer segmental dynamics, crystallinity, ion concentration and their dissociation (see discussion of the FTIR data below), as well as the coordination/mobility of charge carriers [41–43]. The conductivity of plasticized crosslinked PEO shows a higher value than that of plasticized linear PEO (Fig. 4b). To put these membrane conductivity values in perspective, the conductivity of a liquid electrolyte containing 1M NaTf in TEGDME (Figs. 3a and 4b) was also measured, which sets the upper limit of the ionic conductivity of the current polymer membrane system. Compared to 1M NaTf in TEGDME, the plasticized crosslinked PEO exhibits only an order of magnitude lower conductivity. Since most polymeric systems typically result in several orders of magnitude lower conductivity than their liquid counterparts, this plasticized crosslinked PEO presents significant promise toward maintaining high ionic conductivity.

3.4. *Thermal and electrochemical stability of NaTf PEGDGE/Jeffamine membranes*

The thermal stability of the crosslinked PEO membrane was evaluated by a flame retardation test and TGA (Fig. 5). The crosslinked PEO membrane was exposed to an open flame where it remained intact and dimensionally stable for 35 s before ignition. For comparison, a commercial Celgard® separator melted within 5 s under the same test conditions (video provided in supplemental information). TGA analysis of dry crosslinked PEO shows that the polymer has only a 2% weight loss up to 350 °C, while the plasticized membrane shows TEGDME evaporation occurring at 200 °C, consistent with a report by Carbone et al. who studied the electrochemical and thermal properties of various ether-based/LiTf electrolytes [7]. Linear sweep voltammetry was used to evaluate the electrochemical stability window of non-plasticized and plasticized membranes at 40 °C (Fig. 6a). The onset of oxidative degradation occurs at 4.5 V vs. Na/Na^+ for non-plasticized crosslinked PEO and 3.8 V vs. Na/Na^+ for TEGDME plasticized crosslinked PEO, with both having an oxidative threshold value of 5.5 V. Reports indicate that for lithium systems, TEGDME has an oxidative degradation onset of 4.5 V vs. Li/Li^+ [7] and can even improve the oxidative onset point in PEO-based polymer electrolytes [20].

Supplementary video related to this article can be found at https://do

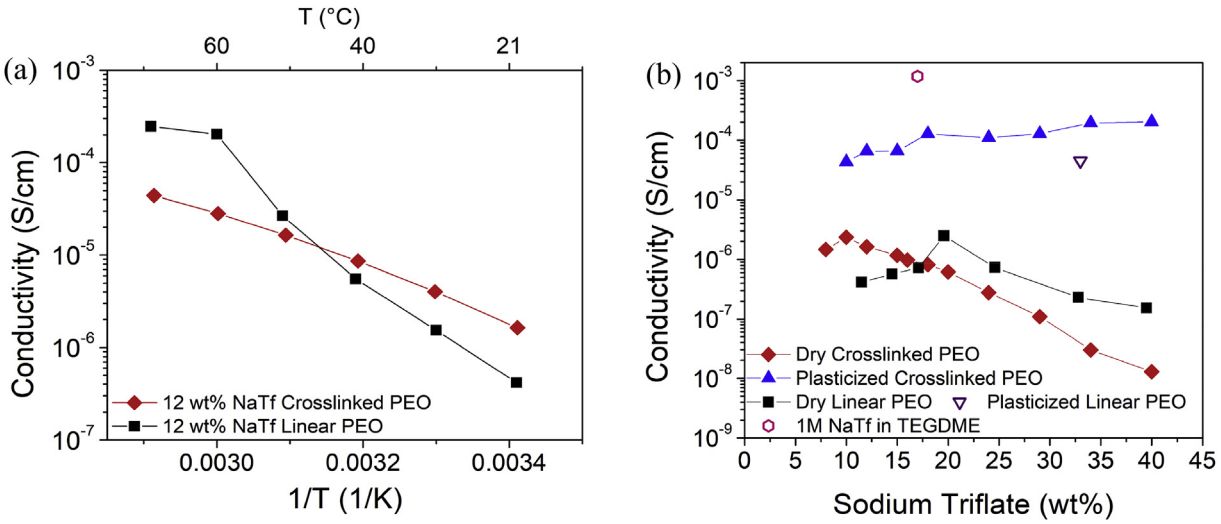

Fig. 4. (a) Conductivity of dry 12 wt% NaTf linear PEO and crosslinked PEO from 70 °C to 20 °C. (b) Comparison of conductivity as a function of wt% NaTf at 20 °C for non-plasticized and plasticized crosslinked PEO, linear PEO, and 1 M NaTf in TEGDME.

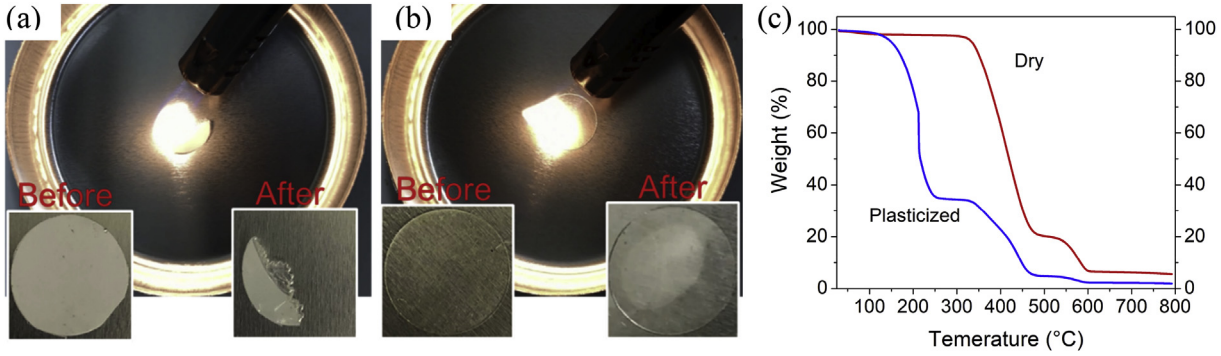

Fig. 5. Thermal stability test of (a) Celgard® commercial separator after 10 s exposure to open flame. (b) Crosslinked PEO after 15 s exposure to open flame, with moisture from the aluminum pan observed. (c) TGA analysis of non-plasticized and plasticized crosslinked PEO.

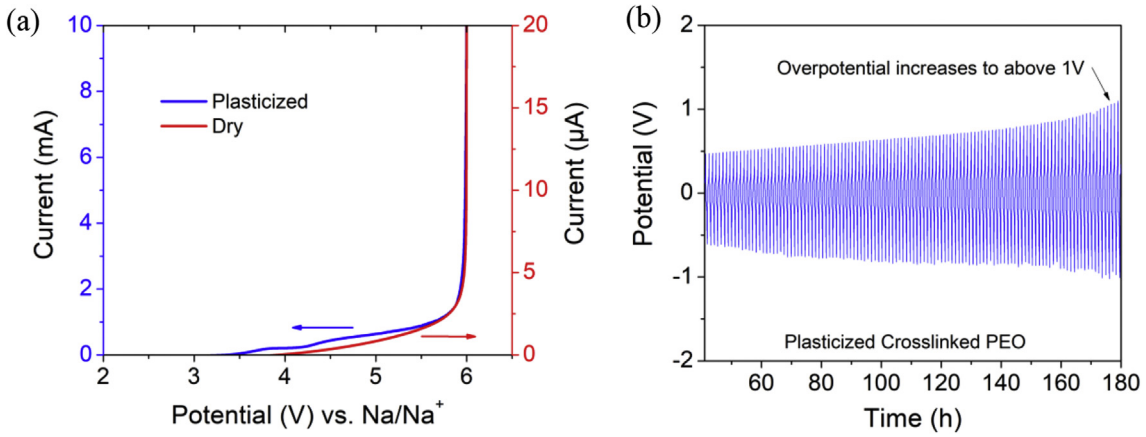

Fig. 6. (a) Linear sweep voltammetry of 18 wt% NaTf non-plasticized and plasticized crosslinked PEO. (b) Potential verses time test of sodium stripping and plating in sodium foil symmetric cell for 18 wt% NaTf plasticized crosslinked PEO.

i.org/10.1016/j.ensm.2019.06.028.

The electrochemical performance of the membranes is further tested by sodium stripping and plating in a sodium foil symmetric cell at a current density of 73 μA/cm^2 (Fig. 6b). The plasticized membrane can effectively cycle sodium metal, though a steady increase in the overpotential is observed. This could be an indication that a resistive solid-electrolyte interphase (SEI) layer is formed [44], or that contact between the sodium metal and membrane decreases over time (see Fig. 7 and discussion below). After 180 h and a charge of 47.3 C/cm^2, the overpotential increases above 1 V, but there is no indication of short circuit by Na dendrites. Linear PEO failed due to sodium dendrite penetration after just 23 h, with a total charge passed of 3.1 C/cm^2 [17], and PVDF-HFP failed after 80 h with a charge of 28.8 C/cm^2 [45].

The surface morphology of the Na anode after the stripping/plating

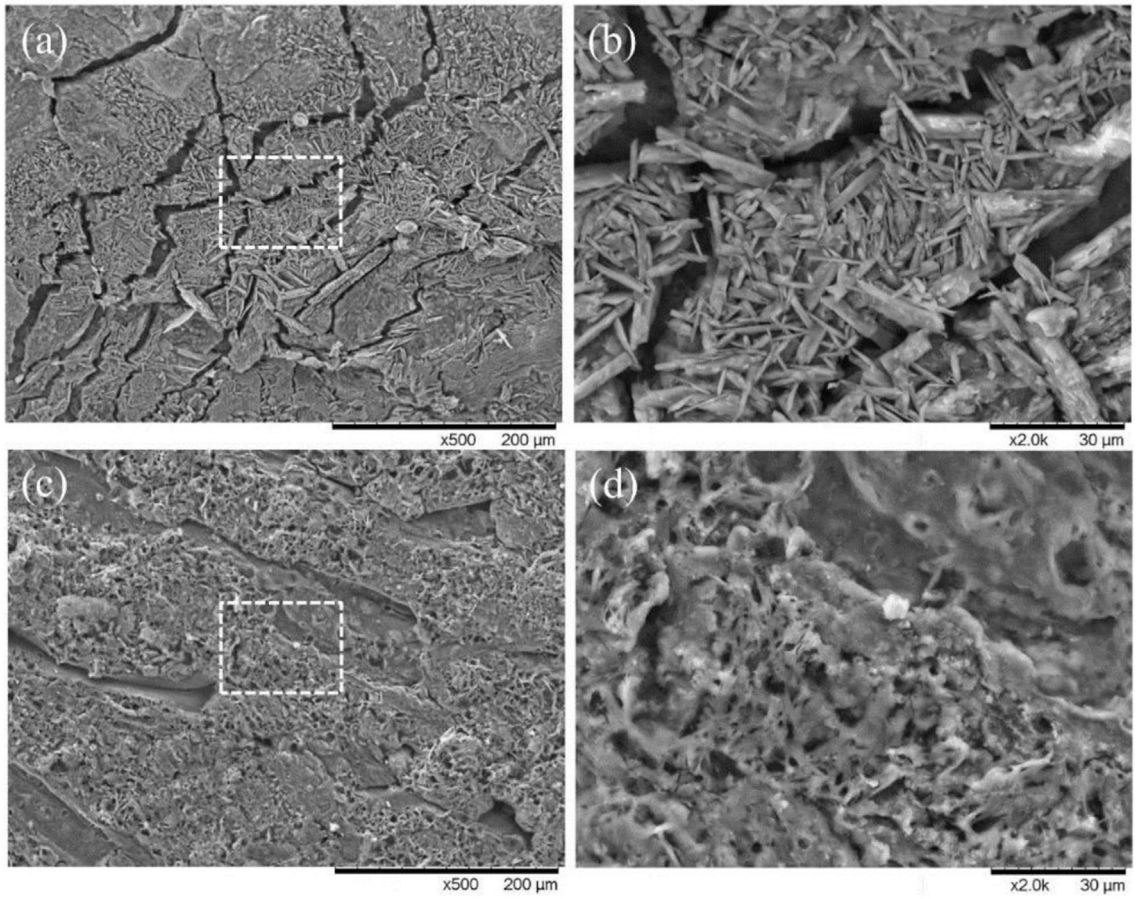

Fig. 7. SEM micrographs of the Na metal anode after stripping/plating tests for 18 wt% NaTf linear and crosslinked PEO. (a) Surface morphology of the Na anode taken from a Na | linear PEO membrane | Na cell. (b) Magnified SEM image from the region labeled by a white box in (a). (c) Surface morphology of the Na anode taken from a Na | plasticized crosslinked PEO membrane | Na cell. (d) The magnified SEM image from the region labeled by a white box in (c).

test was explored by SEM for both crosslinked PEO and linear PEO. Two different and distinct morphologies were observed on the Na surface in contact with linear PEO and plasticized crosslinked PEO. The morphology of the former, as shown in Fig. 7a and b are fully developed dendrites, quite similar to what was observed in a similar study by Stark et al. [46]. In contrast, the Na metal anode taken from the crosslinked PEO symmetric cell exhibits a sponge-like pattern, possibly formed by underdeveloped dendrites and uneven plating of Na. The resultant porous structure caused the Na anode to lose contact with the crosslinked membrane over time, leading to an increase in the overpotential as seen in the stripping/plating test (Fig. 6b). This conclusion is further supported by the finding that less of an SEI layer is observed on the Na anode for the crosslinked PEO membrane as compared to its linear PEO counterpart (Fig. S5).

The transference number of Na^+ (t_c) was evaluated using both the diffusion coefficients determined by NMR and the Bruce-Vincent method [47,48] for non-plasticized and plasticized crosslinked PEO membranes, given by the following formulas:

Na^+ ion transference number, $t_{c(NMR)}$ from the diffusion coefficients determined by NMR:

$$t_{c(NMR)} = \frac{D^+_{NMR}}{D^+_{NMR} + D^-_{NMR}} \tag{3}$$

where D^+_{NMR} and D^-_{NMR} are the Na^+ cation and Tf^- anion diffusivities, respectively.

Bruce-Vincent:

$$t_{c(BV)} = \frac{I_{ss}(\Delta V - I_0 R_0)}{I_0(\Delta V - I_s R_{ss})} \tag{4}$$

where I_0 and I_{ss} are the initial and steady-state currents (Fig. 8a); ΔV is the bias voltage, set as 7.5 mV; R_0 and R_{ss} are the initial and steady-state interfacial resistances, which were obtained by electrochemical impedance spectra at open circuit voltage before and after applying the bias potential (Fig. 8b and c).

The relaxation times (T_1 and T_2), rotational correlation time (τ_c) and estimated diffusion coefficients (D_{NMR}) for Na^+ cation and Tf^- anion for the crosslinked PEO membranes obtained from NMR are summarized in Table S3. As can be seen from Table S3, the relaxation time is too short to apply pulse field gradient (PFG) NMR to these samples, except for the Tf^- anion in the plasticized sample. Thus, for the plasticized sample, the Tf^- anion diffusion coefficient was determined both from rotational correlation time, τ_c using Equation S(1) and ^{19}F PFG-NMR. PFG-NMR gives a Tf^- anion diffusion coefficient of $D_{PFG} = 9.0 \times 10^{-12}$ m^2/s, which is in reasonable agreement with $D^-_{NMR} = 2.13 \times 10^{-11}$ m^2/s, estimated from τ_c. Thus, it is believed that the diffusion coefficients estimated from τ_c are useful to calculate the Na^+ ion transference numbers ($t_{c(NMR)}$). As seen in Fig. 8d, the value obtained by the Bruce-Vincent method at 20 °C for the plasticized membrane is higher than that obtained from NMR relaxation time measurements. We attempted to obtain a value for the dry membrane using the Bruce-Vincent method at 20 °C, but due to the high resistance of the membrane, the steady state current was too noisy to obtain a reliable value.

To determine the expected agreement of t_c between the Bruce-Vincent method and NMR relaxation time measurements, an ideality parameter (β) can be applied, given by the formula [49]:

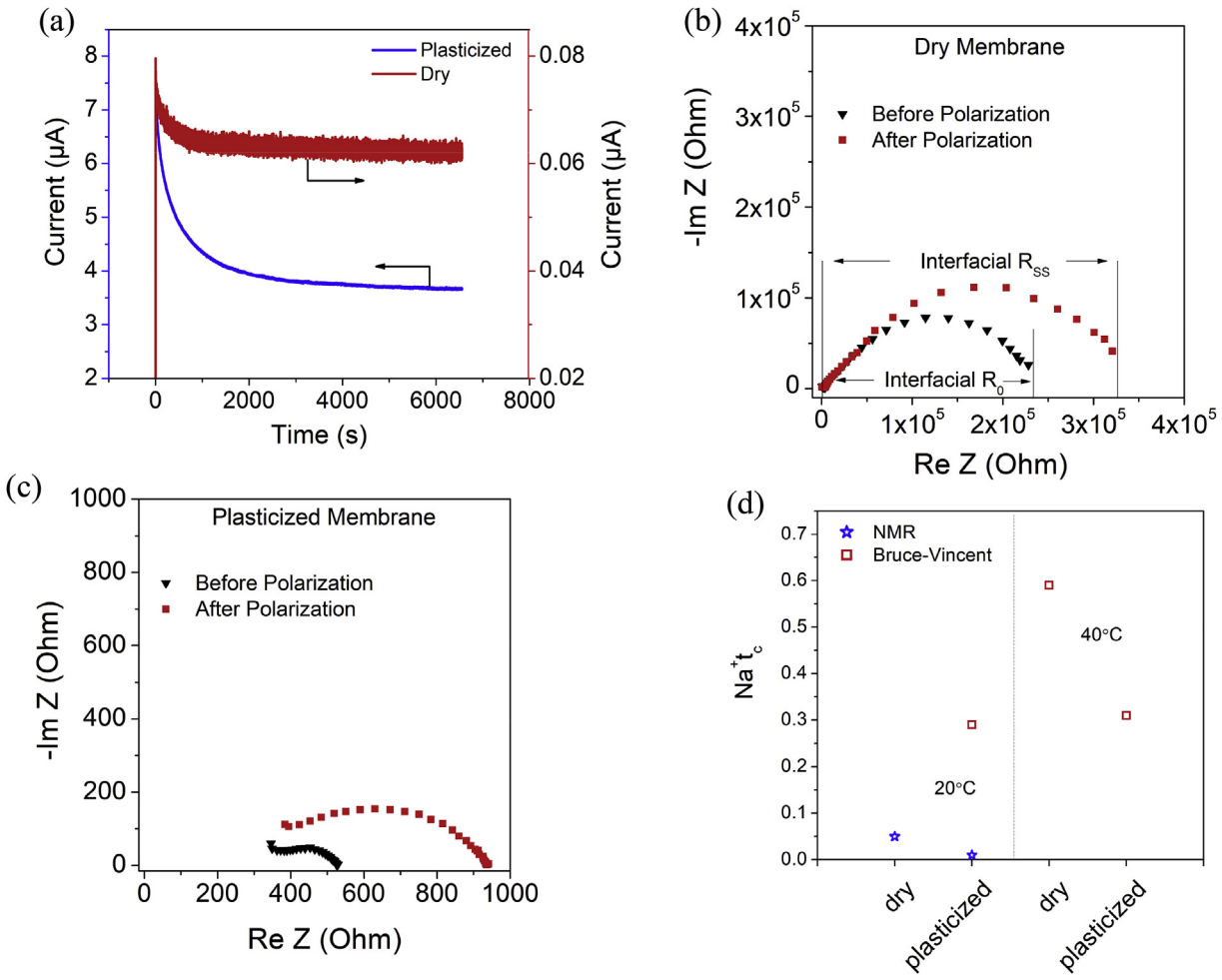

Fig. 8. (a) Current decay over time after applying a bias potential of 7.5 mV. (b) Electrochemical impedance of non-plasticized crosslinked PEO before and after bias potential is applied. (c) Electrochemical impedance spectroscopy of TEGDME plasticized crosslinked PEO before and after bias potential is applied. (d) Transference number for dry and plasticized crosslinked PEO measured by NMR and Bruce-Vincent methods.

$$\beta = \frac{\sigma RT}{F^2 c \left(D^+_{NMR} + D^-_{NMR}\right)} \quad (5)$$

where σ is the ionic conductivity, R is the gas constant, T is temperature, F is Faraday's constant, and c is the bulk molar salt concentration. A β value close to 1 indicates that a good agreement is expected for transference numbers obtained from NMR and galvanostatic polarization methods, while a $\beta < 1$ indicates the values are expected to be different. The ideality parameter provides a measure of how much the diffusivities, D^+ and D^-, obtained by NMR relaxation time measurements are due to disassociated ions (β close to 1) or a combination of associated and disassociated ions ($\beta < 1$), which results in a lower self-diffusion value by NMR than that of the charged species diffusivity measured by galvanostatic methods. The calculated β value for the dry membranes is 0.006 and 0.174 for the plasticized membrane (Table S4). This indicates that we should not expect reasonable agreement between the two methods. The t_c value (0.3) of the plasticized membranes measured at 20 °C and 40 °C by the Bruce-Vincent method are in reasonable agreement with those typically reported for linear PEO (t_c, 0.2–0.5) [47,50,51]. An interesting finding is that t_c decreases upon plasticization (Fig. 8d) by both NMR and Bruce-Vincent methods. The higher t_c value for the dry membrane may be due to the crosslinked 3D network restricting triflate anion migration. The decrease in transference number with plasticization indicates that the addition of TEGDME to the polymer matrix changes the mechanism of ion transport. Adding TEGDME provides improved solvation and diffusivity of both ions (confirmed by IR (Fig. 9) and decreased T_g of the matrix (Fig. 2c)), resulting in an increase in ion conductivity (Fig. 3a), but migration of the larger triflate ion is increased to a greater extent than the cation (Table S3).

3.5. FTIR spectra of NaTf PEGDGE/Jeffamine membranes

Vibrational spectroscopy provides an additional means to understand the effect of NaTf coordination chemistry on T_g and ionic conductivity of the membranes. FTIR spectra were acquired for non-plasticized and plasticized crosslinked membranes at various NaTf concentrations. The vibrational modes of the triflate anion are sensitive to changes in coordination, and the FTIR spectra in Fig. 9a and b shows that the degree of ion association increases with NaTf concentration, as expected. The CF_3 in-plane bending mode, δ_s CF_3, occurs near 753 cm^{-1} for the free anion, 757 cm^{-1} for the ion pair, and 761 cm^{-1} for the triple ion $[Na_2Tf]^+$. δ_s CF_3 shifts to higher frequencies of ≥764 cm^{-1} for more highly associated aggregate species [52,53]. Up to 24 wt% NaTf, the triflate anion appears to exist primarily as the free anion or as ion pairs with weak interactions in the non-plasticized membranes [54]. At higher triflate concentrations, the appearance of a strong band at 767 cm^{-1} is clear evidence for the formation of aggregates. These trends are further confirmed by analysis of the SO_3 asymmetric stretch, ν_s SO_3. The band at 1030 cm^{-1} is assigned to free triflate anions. The band around 1042 cm^{-1} is attributed to triflate anions with higher degrees of cation association and may consist of overlapping contributions from ion pairs, triple ions, and aggregates

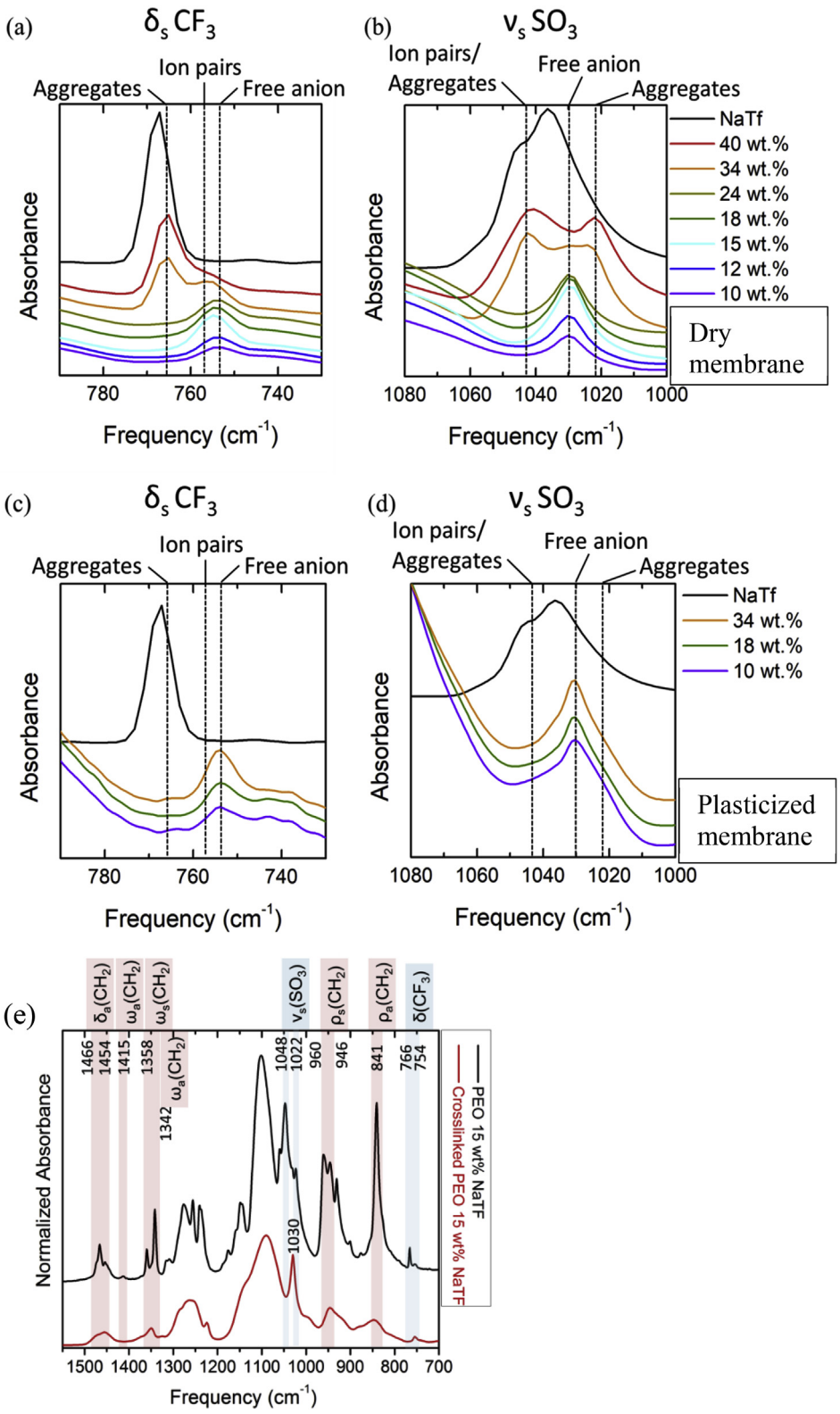

Fig. 9. (a–d) FTIR spectra of plasticized and non-plasticized crosslinked PEO membranes with different wt% NaTf, with pure NaTf shown for comparison. (a,c) Region for CF_3 in-plane bend (δ_s CF_3). (b,d) Region for SO_3 symmetric stretch. (e) Comparison of the FTIR spectra of crosslinked PEO and linear PEO membranes containing 15 wt% NaTf.

[54–56]. The band at 1022 cm^{-1} is attributed to aggregate triflate species [55]. Differences in the free ion concentration within the polymer matrix are one contributing factor to the ionic conductivity of the membranes [57]. The addition of TEGDME to the crosslinked membrane results in a shift of δ_s CF_3 and ν_s SO_3 to 753 cm^{-1} and 1030 cm^{-1}, respectively for the 34 wt% NaTf sample. The shift in δ_s CF_3 and ν_s SO_3 to a lower frequency indicates the presence of free anions (Fig. 9c and d). The disappearance of ν_s SO_3 bands at 1042 cm^{-1} and 1022 cm^{-1} for the 34 wt% NaTf sample is

a clear indication that NaTf preferentially interacts with TEGDME over the polymer chains. The preferential solvation of NaTf by TEGDME is reflected in the almost constant T_g and provides an additional explanation for the significant increase in ionic conductivity of the plasticized membranes.

3.6. FTIR spectral comparison of 15 wt% NaTf linear PEO and PEGDGE/Jeffamine membranes

FTIR also provides an effective means to understand the difference in local chain conformations and NaTf coordination to the polymer backbone between crosslinked PEO and its linear counterpart. This provides insights into the possible differences in ion transport mechanism between the two. The frequency regions masked by blue and red in Fig. 9e represent the characteristic vibrational modes for triflate ion coordination and the PEO chain conformations, respectively.

Intensive work has been done to decipher the conformation of linear PEO using both X-ray analysis and spectroscopic techniques [58–60]. Those early studies show that PEO crystallizes in a helical configuration with a factor group D(4π/7). The helix is constructed with a succession of trans (CCOC), gauche (OCCO), and trans (COCC) conformers (i.e. a tgt conformation) along the helix axis [59]. It has been reported that the coordination of Na^+ by PEO is not expected to distort the backbone conformation [17,61], and this seems to be validated for the linear PEO-NaTf (15 wt%) in this study. As shown in Fig. 9e, the featured band centered at 841 cm^{-1} is ascribed to the asymmetric CH_2 rocking mode for the tgt conformation and the 946 cm^{-1} band represents the tgt symmetric CH_2 rocking mode [58,59]. The band at 1358 cm^{-1} is attributed to the tgt symmetric CH_2 wagging [59]. The intensity of those bands for crosslinked PEO-NaTf (15 wt%) dramatically decreases, indicating fewer tgt conformations of the PEO backbone in crosslinked PEO at room temperature. Hiroatsu et al. attributed the weak band centered at 1415 cm^{-1} to asymmetric CH_2 wagging in the tgt conformation [62], and this mode totally disappears for the crosslinked PEO. This confirms the observation that the tgt conformation is favorable in the linear PEO-NaTf system, but not for crosslinked PEO. The spectrum of crosslinked PEO is analogous to that of molten PEO [63], which has several characteristic modes of the tgg conformation. Broad bands centered at 847, 1352, and 1460 cm^{-1} are assigned to the tgg CH_2 rocking, wagging, and bending modes, respectively [63].

The conformational changes of crosslinked PEO compared to linear PEO may benefit ion dissociation. The NaTf salt in linear PEO forms mainly ion aggregates with a characteristic δ_s CF_3 mode at 766 cm^{-1} [52,53]. The crosslinked PEO with the same salt concentration (15 wt% NaTf) has only a single band centered at 753 cm^{-1}, which is attributed to free anions. This clearly indicates that the portion of ion aggregates decreases in crosslinked PEO. Analysis of the SO_3 symmetric stretch, ν_s SO_3, reinforces this point. For linear PEO, the bands centered at 1022 cm^{-1} and at 1048 cm^{-1} represent triflate aggregates and Na^+ - triflate ion pairs, whereas crosslinked PEO has a single band at 1030 cm^{-1} that is characteristic of free triflate anions.

Our results clearly indicate that the matrix of PEO chain conformations and ion solvation structure are intrinsically different between linear PEO and crosslinked PEO at room temperature. These structural differences are reflected in ionic conductivity. At low salt concentrations, the ionic conductivity of dry crosslinked PEO is ~1 order of magnitude higher than that of linear PEO (Fig. 4b), consistent with the presence of more free ions and fewer ion aggregates.

3.7. Mechanical analysis of crosslinked PEO and linear PEO membranes

Plasticization significantly improves the conductivity of crosslinked and linear PEO, but the plasticized membrane must also exhibit high mechanical stability to be useful in practical devices. Mechanical properties of the non-plasticized and plasticized membranes were evaluated using DMA and rheology, respectively (Fig. 10). Due to the very weak mechanical properties of linear PEO at $T > T_m$ (56 °C), a rheometer was used to accurately measure the modulus of plasticized membranes. Linear PEO exhibited a fairly high modulus at $T < T_m$, but showed a significant decrease in the storage modulus above 56 °C for both non-plasticized and plasticized samples. The low modulus of linear PEO above 56 °C does not provide a stable membrane, preventing its use at operating temperatures above T_m. The presence of a crystalline phase in linear PEO provides a fairly high modulus at low temperatures, but it also inhibits ionic conductivity. The crosslinked membranes show excellent mechanical properties with no significant change in the modulus over the temperature range measured. The modulus for the plasticized crosslinked membrane is maintained at ~1 MPa in the temperature range of -20 – 180 °C, which is a reasonable modulus for a gel polymer electrolyte and sufficiently high for the membrane to be easily handled. Furthermore, the modulus ~1 MPa is a tenfold increase from that in previous reports of plasticized crosslinked membranes [18,40,64]. The stress-strain curve for dry and plasticized membranes is shown in Fig. 10c. The tensile strength of the membranes is 0.924 ± 0.03 MPa and 0.521 ± 0.07 MPa for dry and plasticized membranes respectively (Table 1), consistent with other crosslinked polymer electrolytes [34,65]. The high degree of crosslinking enables good tensile strength while maintaining reasonable ductility, resulting in a Youngs Modulus of 3.41 ± 0.25 MPa and 2.32 ± 0.16 MPa for non-plasticized membranes and plasticized membranes respectively (Table 1). Many prior works on PEO-based crosslinked gel polymer electrolytes did not report the mechanical properties of their membranes [27,29,34,38,66,67], possibly due to the inherently weak nature of gel polymer electrolytes. The mechanical stability and excellent conductivity over a wide temperature range combined with the thermal and electrochemical stability of TEGDME provides a path for a highly conductive membrane that is useful for a variety of battery applications.

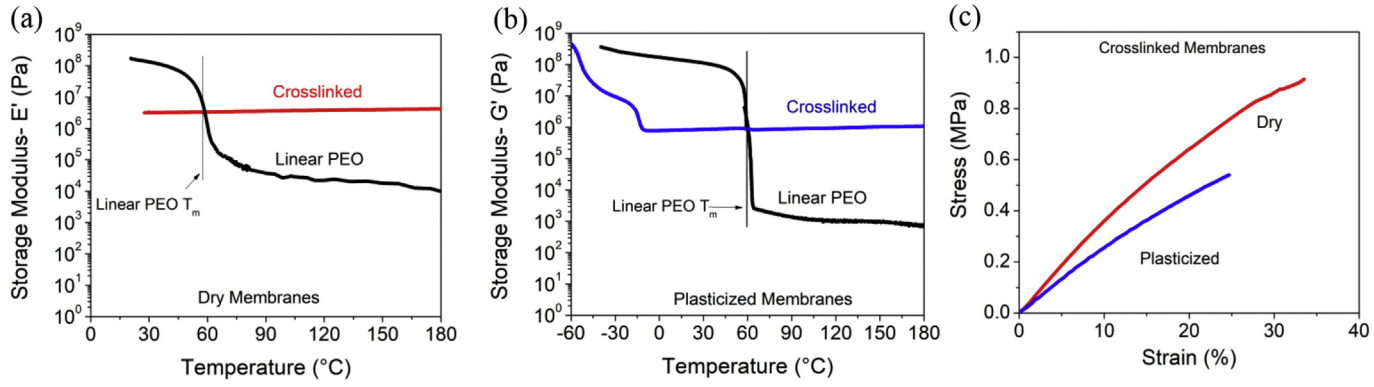

Fig. 10. Mechanical analysis of crosslinked PEO and linear PEO. (a) DMA of non-plasticized membrane. (b) Rheology of TEGDME plasticized membrane. (c) Stress-strain curve of non-plasticized and plasticized crosslinked PEO membranes at 21 °C.

Table 1
Mechanical properties of dry and plasticized 18 wt% NaTf crosslinked PEO membrane at 21 °C.

Sample	Youngs Modulus (MPa)	Tensile Strength (MPa)	Elongation at Break (%)
Dry	3.41 ± 0.25	0.924 ± 0.03	33.0 ± 2.5
Plasticized	2.32 ± 0.16	0.521 ± 0.07	24.3 ± 4.3

4. Conclusions

A robust crosslinked PEO-based membrane has been developed that demonstrates high ionic conductivity and mechanical stability. The crosslinked films were prepared via a single step synthesis of an amine and epoxide-terminated PEO-based precursors with varied NaTf concentrations. T_g of the dry membranes increased with NaTf concentration due to ionic crosslinking between the salt and polymer chains, and this was reflected in a strong decrease in conductivity with increasing salt concentration. Plasticization of the membranes with TEGDME significantly reduced ionic crosslinking within the polymer matrix due to ion solvation, and this correlated with a much lower T_g that is essentially independent of salt concentration. The addition of TEGDME increased the ionic conductivity of the membranes by 4 orders of magnitude to 2×10^{-4} S/cm at 20 °C, just slightly lower than that of a TEGDME-based liquid electrolyte (1×10^{-3} S/cm). The membranes are sufficiently robust to resist short-circuit by sodium dendrites over the course of 180 h when cycled in a Na metal symmetric cell, and have a Na^+ transference number of 0.58 in the dry membranes and 0.31 in plasticized membranes at 40 °C. In addition, the mechanical properties of the crosslinked membrane were maintained with the addition of plasticizer. The membranes were stable over a wide temperature range with a constant storage modulus of ~1 MPa from −20 °C to 180 °C. The excellent mechanical stability of the crosslinked PEO-based membrane combined with the electrochemical and thermal stability of TEGDME provides a highly conductive gel polymer electrolyte suitable for a variety of Na-based electrochemical energy storage applications.

Conflicts of interest

There are no conflicts of interest to declare.

Author contribution

JN and TS formulated the concept and managed the entire project. ML conducted most of the experiments and wrote a manuscript under the guidance of JN and TS. GY conducted linear PEO experiments, designed experiments for IR, LSV, Na stripping/plating and transport number measurements, obtained SEM/EDX images and contributed to writing the manuscript. DG conducted membrane fabrications with ML. ES and FD assisted ML on performing electrochemical tests, and GY and RR conducted FTIR and analyzed the data. BL performed DMA and SG performed rheology under the guidance of APS. KSH conducted solid state NMR experiments. KSH, VM, GY and JN performed NMR data analysis.

Acknowledgements

This work is funded by Dr. Imre Gyuk, Office of Electricity Delivery and Reliability, Department of Energy and the Laboratory Directed Research and Development Program of Oak Ridge National Laboratory, managed by UT-Battelle, LLC. SG, BL, and APS acknowledge partial financial support on DMA and rheology measurements by the U.S. Department of Energy, Office of Science, Basic Energy Sciences, Materials Sciences and Engineering Division. NMR experiments were performed at EMSL, a DOE Office of Science user facility sponsored by the DOE BER and located at PNNL. We also thank Huntsman Corporation for providing us Jeffamine®.

Appendix A. Supplementary data

Supplementary data to this article can be found online at https://doi.org/10.1016/j.ensm.2019.06.028.

References

[1] P. Barpanda, G. Oyama, S. Nishimura, S.C. Chung, A. Yamada, Nat. Commun. 5 (2014) 4358–4366.
[2] Y.M. Li, Y.X. Lu, C.L. Zhao, Y.S. Hu, M.M. Titirici, H. Li, X.J. Huang, L.Q. Chen, Energy Storage Mater 7 (2017) 130–151.
[3] J.B. Goodenough, Energy Storage Mater 1 (2015) 158–161.
[4] H.Y. Che, S.L. Chen, Y.Y. Xie, H. Wang, K. Amine, X.Z. Liao, Z.F. Ma, Energy Environ. Sci. 10 (2017) 1075–1101.
[5] V. Palomares, P. Serras, I. Villaluenga, K.B. Hueso, J. Carretero-Gonzalez, T. Rojo, Energy Environ. Sci. 5 (2012) 5884–5901.
[6] Q.S. Wang, P. Ping, X.J. Zhao, G.Q. Chu, J.H. Sun, C.H. Chen, J. Power Sources 208 (2012) 210–224.
[7] L. Carbone, M. Gobet, J. Peng, M. Devany, B. Scrosati, S. Greenbaum, J. Hassoun, ACS Appl. Mater. Interfaces 7 (2015) 13859–13865.
[8] C. Berthier, W. Gorecki, M. Minier, M.B. Armand, J.M. Chabagno, P. Rigaud, Solid State Ionics 11 (1983) 91–95.
[9] B.L. Papke, M.A. Ratner, D.F. Shriver, J. Phys. Chem. Solids 42 (1981) 493–500.
[10] G. Petersen, P. Jacobsson, L.M. Torell, Electrochim. Acta 37 (1992) 1495–1497.
[11] S.A. Hashmi, S. Chandra, Mat. Sci. Eng. B-Solid 34 (1995) 18–26.
[12] J.S. Moreno, M. Armand, M.B. Berman, S.G. Greenbaum, B. Scrosati, S. Panero, J. Power Sources 248 (2014) 695–702.
[13] S.S. Rao, M.J. Reddy, K.N. Reddy, U.V.S. Rao, Solid State Ionics 74 (1994) 225–228.
[14] D.T. Hallinan, N.P. Balsara, Annu. Rev. Mater. Res. 43 (2013) 503–525.
[15] R. Chandrasekaran, I.R. Mangani, R. Vasanthi, S. Selladurai, Ionics 7 (2001) 94–100.
[16] D.K. Pradhan, B.K. Samantaray, R.N.P. Choudhary, N.K. Karan, R. Thomas, R.S. Katiyar, Ionics 17 (2011) 127–134.
[17] R.E. Ruther, G. Yang, F.M. Delnick, Z.J. Tang, M.L. Lehmann, T. Saito, Y.J. Meng, T.A. Zawodzinski Jr., J. Nanda, ACS Energy Lett 3 (2018) 1640–1647.
[18] R. Khurana, J.L. Schaefer, L.A. Archer, G.W. Coates, J. Am. Chem. Soc. 136 (2014) 7395–7402.
[19] D. Luo, Y. Li, M.J. Yang, Mater. Chem. Phys. 125 (2011) 231–235.
[20] L. Porcarelli, C. Gerbaldi, F. Bella, J.R. Nair, Sci Rep-Uk 6 (2016) 1–14.
[21] V. Chaudoy, F.T. Van, M. Deschamps, F. Ghamouss, J. Power Sources 342 (2017) 872–878.
[22] C.-H. Tsao, Y.-H. Hsiao, C.-H. Hsu, P.-L. Kuo, ACS Appl. Mater. Interfaces 8 (2016) 15216–15224.
[23] J.F. Lenest, S. Callens, A. Gandini, M. Armand, Electrochim. Acta 37 (1992) 1585–1588.
[24] X.G. Sun, C.L. Reeder, J.B. Kerr, Macromolecules 37 (2004) 2219–2227.
[25] M. Watanabe, A. Nishimoto, Solid State Ionics 79 (1995) 306–312.
[26] Y. Aihara, J. Kuratomi, T. Bando, T. Iguchi, H. Yoshida, T. Ono, K. Kuwana, J. Power Sources 114 (2003) 96–104.
[27] H.C. Gao, W.D. Zhou, K. Park, J.B. Goodenough, Adv. Energy Mater. 6 (2016) 1–8.
[28] F. Colo, F. Bella, J.R. Nair, C. Gerbaldi, J. Power Sources 365 (2017) 293–302.
[29] F. Bella, F. Colo, J.R. Nair, C. Gerbaldi, ChemSusChem 8 (2015) 3668–3676.
[30] Z.W. Seh, J. Sun, Y.M. Sun, Y. Cui, ACS Cent. Sci. 1 (2015) 449–455.
[31] V.C. Nogueira, C. Longo, A.F. Nogueira, J. Photochem. Photobiol. A Chem. 181 (2006) 226–232.
[32] W.R. Carper, C.E. Keller, J. Phys. Chem. A 101 (1997) 3246–3250.
[33] W.R. Carper, G.J. Mains, B.J. Piersma, S.L. Mansfield, C.K. Larive, J. Phys. Chem. 100 (1996) 4724–4728.
[34] R.X. He, T. Kyu, Macromolecules 49 (2016) 5637–5648.
[35] J. Kriz, S. Abbrent, J. Dybal, D. Kurkova, J. Lindgren, J. Tegenfeldt, A. Wendsjo, J. Phys. Chem. A 103 (1999) 8505–8515.
[36] J.K. Kim, Y.J. Lim, H. Kim, G.B. Cho, Y. Kim, Energy Environ. Sci. 8 (2015) 3589–3596.
[37] D.T. Hallinan, I. Villaluenga, N.P. Balsara, MRS Bull. 43 (2018) 759–767.
[38] N. Paranjape, P.C. Mandadapu, G. Wu, H.Q. Lin, Polymer 111 (2017) 1–8.
[39] A. Thiam, C. Antonelli, C. Iojoiu, F. Alloin, J.Y. Sanchez, Electrochim. Acta 240 (2017) 307–315.
[40] Q. Zheng, L. Ma, R. Khurana, L.A. Archer, G.W. Coates, Chem. Sci. 7 (2016) 6832–6838.
[41] D.K. Pradhan, B.K. Samantaray, R.N.P. Choudhary, A.K. Thakur, J. Power Sources 139 (2005) 384–393.
[42] Q. Ma, J.J. Liu, X.G. Qi, X.H. Rong, Y.J. Shao, W.F. Feng, J. Nie, Y.S. Hu, H. Li, X.J. Huang, L.Q. Chen, Z.B. Zhou, J. Mater. Chem. 5 (2017) 7738–7743.
[43] F. Alloin, J.Y. Sanchez, M. Armand, J. Electrochem. Soc. 141 (1994) 1915–1920.
[44] X.B. Cheng, R. Zhang, C.Z. Zhao, Q. Zhang, Chem. Rev. 117 (2017) 10403–10473.
[45] W.D. Zhou, Y.T. Li, S. Xin, J.B. Goodenough, ACS Cent. Sci. 3 (2017) 52–57.
[46] J.K. Stark, Y. Ding, P.A. Kohl, J. Electrochem. Soc. 158 (2011) A1100–A1105.
[47] J. Evans, C.A. Vincent, P.G. Bruce, Polymer 28 (1987) 2324–2328.
[48] A.S. Pandian, X.C. Chen, J.H. Chen, B.S. Lokitz, R.E. Ruther, G. Yang, K. Lou, J. Nanda, F.M. Delnick, N.J. Dudney, J. Power Sources 390 (2018) 153–164.
[49] M. Chintapalli, K. Timachova, K.R. Olson, S.J. Mecham, D. Devaux, J.M. DeSimone, N.P. Balsara, Macromolecules 49 (2016) 3508–3515.
[50] C.M. Ma, Z.P. Mao, J. Zhou, J. Yan, Chin. Phys. 5 (1985) 664–668.

[51] K. Pozyczka, M. Marzantowicz, J.R. Dygas, F. Krok, Electrochim. Acta 227 (2017) 127–135.
[52] H.T. Dong, J.K. Hyun, C.P. Rhodes, R. Frech, R.A. Wheeler, J. Phys. Chem. B 106 (2002) 4878–4885.
[53] R. Frech, C.P. Rhodes, S.S. York, Solid State Ionics 548 (1999) 335–345.
[54] J. Manning, R. Frech, Polymer 33 (1992) 3487–3494.
[55] C.P. Rhodes, R. Frech, Solid State Ionics 121 (1999) 91–99.
[56] C.P. Rhodes, M. Khan, R. Frech, J. Phys. Chem. B 106 (2002) 10330–10337.
[57] L.M. Torell, P. Jacobsson, G. Petersen, Polm. Adv. Technol. 4 (1993) 152–163.
[58] T. Yoshihara, H. Tadokoro, S. Murahashi, J. Chem. Phys. 41 (1964) 2902–2911.
[59] J. Maxfield, I. Shepherd, Polymer 16 (1975) 505–509.
[60] B. Papke, M. Ratner, D. Shriver, J. Phys. Chem. Solids 42 (1981) 493–500.
[61] C.P. Rhodes, R. Frech, Solid State Ionics 121 (1999) 91–99.
[62] H. Matsuura, T. Miyazawa, J. Polym. Sci. A-2: Polym. Phys. 7 (1969) 1735–1744.
[63] J. Koenig, A. Angood, J. Polym. Sci. A-2: Polym. Phys. 8 (1970) 1787–1796.
[64] J. Shim, L. Kim, H.J. Kim, D. Jeong, J.H. Lee, J.C. Lee, Polymer 122 (2017) 222–231.
[65] Y.K. Kang, K. Cheong, K.A. Noh, C. Lee, D.Y. Seung, J. Power Sources 119 (2003) 432–437.
[66] G.T. Kim, G.B. Appetecchi, M. Carewska, M. Joost, A. Balducci, M. Winter, S. Passerini, J. Power Sources 195 (2010) 6130–6137.
[67] B. Rupp, M. Schmuck, A. Balducci, M. Winter, W. Kern, Eur. Polym. J. 44 (2008) 2986–2990.